Received: 18 December 2019 | Revised: 8 April 2020 | Accepted: 13 May 2020

DOI: 10.1002/ese3.759

Energy Science & Engineering
Open Access

RESEARCH ARTICLE

Evaluation of elastoplastic properties of brittle sandstone at microscale using micro-indentation test and simulation

Rui Song[1,2] | **Yao Wang**[3] | **Shuyu Sun**[2] | **Mengmeng Cui**[3] | **Jianjun Liu**[1]

[1]State Key Laboratory of Geomechanics and Geotechnical Engineering, Institute of Rock and Soil Mechanics, Chinese Academy of Sciences, Wuhan, China

[2]Computational Transport Phenomena Laboratory (CTPL), King Abdullah University of Science and Technology (KAUST), Thuwal, Saudi Arabia

[3]Southwest Petroleum University, Chengdu, China

Correspondence
Shuyu Sun, Computational Transport Phenomena Laboratory (CTPL), King Abdullah University of Science and Technology (KAUST), Thuwal 23955-6900, Saudi Arabia.
Email: shuyu.sun@kaust.edu.sa

Mengmeng Cui, Southwest Petroleum University, Chengdu 610500, China.
Email: cuimm619@163.com

Funding information
Financial support of King Abdullah University of Science and Technology (KAUST), Grant/Award Number: BAS/1/1351-01 ; National Natural Science Foundation of China, Grant/Award Number: 51909225 and 51874262; State Key Laboratory of Geomechanics and Geotechnical Engineering, Grant/Award Number: Z017009; National Science and Technology Major Project of China, Grant/Award Number: 2017ZX05013001-002; China Scholarship Council

Abstract

The micro-indentation test has been regarded as an efficient tool to obtain the elasticity modulus and hardness of the minerals in rock, which is essential for studying the deformation-crack mechanism of the pore structure. However, researches on microscopic plastic parameters have been rarely conducted. This paper develops a novel method to determine the microscopic initial strength and residual strength of brittle sandstone. A dimensionless analysis on the micro-indentation curve of rock is conducted to acquire its key influencing factors of the elastoplastic properties, which include the initial cohesive force and the residual cohesive force. Then, small cylindrical rock samples are prepared for micro-CT scanning and micro-indentation test by a conical indenter to acquire the microstructure, indentation curve, and the microscale elasticity. The pore scale indentation simulation is conducted using the reconstructed rock models with different strength. The function between the indentation curve and strength is deduced by the parametric finite element method (FEM) study. Based on this function, the microscale initial strength and residual strength of the brittle sandstone are determined. The proposed method is validated by comparing the microscale numerical simulation results of uniaxial compression on the representative volume element (RVE) model of rock with the experimental results. A reasonable deviation is observed compared with the experimental benchmark data for the stress-strain curves, as well as Young's modulus and uniaxial compression strength, proving the effectiveness of the proposed method.

KEYWORDS

dimensionless analysis, initial strength, micro-CT, micro-indentation, residual strength

1 | INTRODUCTION

Sandstone is one of the most important types of sedimentary rock, mainly composed of quartz or feldspar. It is widely applied in geotechnical engineering, such as the underground construction, dam base rock, and tunneling. Thus, numerous scientific efforts have been devoted to studying the time-dependent deformation, failure characteristics, and strength

in the uniaxial/triaxial compression and tension tests.[1-3] Furthermore, sandstones make up about 50%-60% of reservoirs in the world,[4,5] the tiny pore structures of which are the main storage space and flow channel for oil and gas. The requirements for enhancing oil recovery (EOR) advance the study on the transport properties of pore scale fluids, which are also beneficial to CO_2 geological sequestration and underground contaminant control.[6-8] In this case, the mechanical response of rock at the microscale is crucial to the deformation-crack mechanism of the pore structure. Using the reconstructed rock models of micro-X-ray computerized tomography (CT) images, Ju et al,[9] Liu et al,[10] and Zhou and Xiao[11,12] analyzed the pore scale deformation-failure mechanism of rock under the stress wave propagation or in the uniaxial/triaxial compression. Song et al[13] established a structured mesh model of sandstones by micro-CT images and simulated the evolution of pore structure and the permeability of rock. However, the mechanical properties of rock used for the pore scale samples (usually about 1 mm in length) in the above studies are all obtained from the standard cylindrical samples (25 or 50 mm in diameter, and 50 or 100 mm in height). The laboratory test on the microscale mechanical properties of rock is challenged by the sample preparation, the measurement accuracy, and the size limitations for sample holder of the equipment.[14,15] Nevertheless, the pore scale study on the deformation-crack mechanism of rock requires the input mechanical parameters at the same scale, which have not been addressed in literature to our knowledge. Thus, this paper aims to propose a novel method to evaluate the microscale elastoplastic properties of rock using the micro-indentation test and simulations.

For decades, plenty of indentation tests have been conducted to characterize rock properties and the mechanical response at drilling and excavation processes (eg, rock fracture and fragmentation). The indenter types include cylinder,[16] wedge, cone,[17] and hemispherical shapes.[18] The sizes of indenters used in the rock indentation tests range from 3 to 20 mm in diameter.[19] Many studies have been devoted to the indentation fracture zone where the shape of a truncated ellipsoid is assumed, including the elastic zone; the inelastic zone; the cracked zone; and the crushed zone.[16,20] Ladanyi[21] found that the diameter of the crushed zone in sandstone with a porosity of 8.6% is about 20% larger than that of the indenter. Jeng et al[22] observed that the particle size of gypsum samples in the crushed zone is much smaller than that of the intact rock. Yagiz and Rostami[23] measured the rock brittleness using the indentation test. The acoustic emission (AE) and digital image technique were used to characterize the distribution and evolution mechanism of microcrack in the indentation test.[24-27] The correlations between indentation parameters and the elastic modulus of different kinds of rock have been developed based on the experimental results.[28,29] Besides, many scientific efforts have been made to simulate the quasi-static indentation processes of rock combining FEM,[30] displacement discontinuity method (DDM),[31] or discrete element modeling (DEM)[32] with different constitutive law of rock, for example, the linear Mohr-Coulomb, Drucker-Prager, and damage model.[33,34] However, the indenter size adopted in these studies is in the millimeter scale, in which case the rock samples is assumed as intact, isotropic, and homogeneous. Accordingly, the spatial distributions of pore structure and minerals have been ignored.

With the developments of advanced instruments and characterization techniques, the high spatial resolution of micro-/nano-indentation makes it possible to establish the link between the mineralogy/morphology and the mechanical properties in multiphase materials.[35,36] Wang et al,[37] Auvray et al,[38] and Han et al[39] obtained the microscale elastic modulus and hardness of different rock by micro-indentation tests. Using the nano-indentation test with higher resolution than micro-indentation, Zhu et al[40] and Daphalapurkar et al[41] acquired Young's modulus, hardness, and fracture toughness of the individual mineral phases of cement paste and natural rock. Goodarzi et al[42] predicted the elastic response of realistic shale models with homogenization techniques and verified the feasibility by comparing with published results of indentation tests. However, most literatures have been focused on the elasticity and hardness of rock samples, while the microscopic plastic parameters are rarely studied, which are the focus of this research.

This paper develops a novel method to determine the microscopic initial strength and residual strength of brittle sandstone. A dimensionless analysis on the micro-indentation curve of rock is conducted to acquire the key influencing factors of elastoplastic properties. Then, small cylindrical rock samples are prepared for micro-CT scanning and micro-indentation test using a conical indenter to acquire the microscale structure, indentation curve, and the microscale Young's modulus. The pore scale indentation simulation is conducted by ANSYS using the constructed rock models with different strength. The function between the indentation curve and strength is deduced by the parametric FEM study. Using this function, the microscale initial strength and residual strength of the brittle sandstone are determined. This determination method is validated by comparing the microscale numerical simulation results of uniaxial compression on the RVE of rock with the experimental results.

2 | METHODS AND SAMPLE

This section presents the evaluation methodology of microscale elastoplastic properties of brittle sandstone using micro-indentation test and simulation.

2.1 | Indentation tests

The schematic of micro-indentation test is conducted using the conical indenter with a flat tip, and a typical indentation loading-unloading curve is presented in Figure 1. Based on the relationship between the indentation parameters and Young's modulus, the reduced Young's modulus, E_r, is determined by,[43,44]

$$E_r = \frac{S\sqrt{\pi}}{2\sqrt{A_c}} \tag{1}$$

where A_c is the contact area between the tip and the tested sample.

For the conical indenter with a flat punch used in this paper,[45] the contact area is expressed as,

$$A_c = \pi\left(R_{co} + h_c \tan\frac{\alpha}{2}\right)^2 \tag{2}$$

where R_{co} is the radius of the flat tip of the conical indenter, α is the angle of the conical tip, and h_c is the indentation contact depth, which can be calculated by,

$$h_c = h_m - \varepsilon\frac{P_{\max}}{S} \tag{3}$$

where ε is the geometry constant of the tip and h_m the maximum depth. For the conical tip, $\varepsilon = 0.72$. S is the stiffness, which can be calculated by:

$$S = \left.\frac{dP}{dh}\right|_{h=h_m} \tag{4}$$

Then, Young's modulus of the tested sample (E_r) can be determined by,

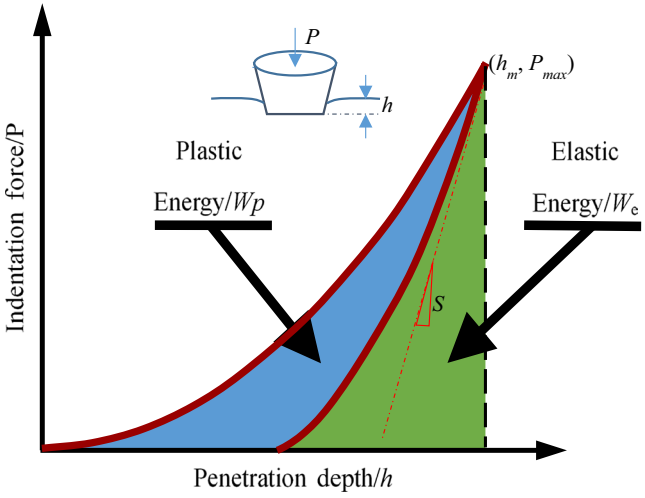

FIGURE 1 Schematic of indentation loading and unloading curve

$$\frac{1}{E_r} = \frac{1-\nu_s^2}{E_s} + \frac{1-\nu_1^2}{E_1} \tag{5}$$

where E is Young's modulus, and ν is Poisson's ratio, where the subscript of s and 1 represents the parameter of the tested sample and the indenter, respectively.

2.2 | Dimensionless analysis

The dimensionless analysis on the micro-indentation curve of rock is conducted to determine the key influencing factors of the elastoplastic properties, including the initial cohesive force and the residual cohesive force. Previous studies have been conducted to characterize the elastoplastic relationship of the indentation curve (Figure 1)[45-47] using the shape functions Π_i, for example, the total energy during loading, W (the area under the loading curve), the maximum force, P_m, the unloading slope, S, the elastic energy, W_e (the area under the unloading curve), and the residual or final depth, h_f. The basic form of the shape function can be written as,

$$\prod_i = F_i(E, f_p, \alpha, h, R, f_{pore}) \tag{6}$$

where the total energy W is used in this study, which is defined as,

$$W = \int_0^{h_{\max}} F dh = W_e + W_p \tag{7}$$

where the impact factor of W in the indentation curve includes the elasticity E and the plastic criterion of the tested material (f_p); the impact factor of pore structure at the contact zone, f_{pore}; the indentation depth h; the conical angle (α); and radius of the flat tip (R).

The microscale sandstone skeleton is assumed as isotropic and homogeneous with perfectly elastic-plastic behavior. And the linear Mohr-Coulomb yield criterion is adopted in this study,

$$\tau_n = C + \sigma_n \tan\varphi \tag{8}$$

where τ_n and σ_n are the shear stress and normal stress, respectively; C and φ are the cohesive and friction angle, respectively.

The residual strength of the sandstone after reaching the compressive strength is determined by the residual cohesive (C_r) and friction angle (φ_r). The cohesion weakening and friction strengthening phenomenon are adopted, which has been validated by many scholars.[48,49] In this theory, the increasing of microcrack leads to the decrease of the cohesive strength. But the frictional strength appears after crack and increases

after broken into the finer rock fragmentation. Thus, the microscopic residual friction angle is considered to be constant to the initial friction angle, which is determined by the lab test. Thus, Equation (6) can be expressed as,

$$W = F_i(E, C, C_r, \alpha, h, R, f_{pore}) \tag{9}$$

The conical angle and the radius of the flat tip adopted in this study are 60° and 100 μm. The impact factor of pore structure at the contact zone, f_{pore}, is determined by the micro-CT imaging of the indentation sample and its reconstructed model. The modeling details are presented in Section 3. Thus, f_{pore} can be removed from Equation (9). Meanwhile, by applying the dimensional analysis to Equation (9) using Buckingham's PI theorem,[50] it can be simplified as:

$$\frac{W}{Ch^3} = F_i\left(\frac{C}{E}, \frac{C_r}{C}, \frac{h}{R}\right) \tag{10}$$

In this study, two distinct penetration depth of 10 μm and 15 μm are adopted, corresponding to $h/R = 0.1$ and 0.15. For a specific conical indenter, the radius of the flat tip is known. Thus, the term h/R is removed and Equation (10) can be expressed for the specific depth:

$$\frac{W\left|\frac{h}{r} = 0.1 \text{ or } 0.15\right.}{Ch^3} = F_i\left(\frac{C}{E}, \frac{C_r}{C}\right) \tag{11}$$

where E is determined by Equation (1). Since there are two unknown material properties (C, C_r) left in Equation (11), two shape functions at $h/R = 0.1$ and 0.15 are sufficient to determine the properties of the tested material uniquely.

2.3 | Evaluation methodology

Taking sample S1 as an example, the detailed determination procedure of microscale initial strength and residual strength for the brittle sandstone is explained as follows:

(1) Samples preparation and experiment

The small cylinder rock samples with the diameter of 5 mm (shown in Figure 2A) are drilled from the original rock and then dried at 65°C for 12 hours. The top surfaces of the samples are polished for indentation rest using the Triple Ion Beam Cutter produced by Leica EM TIC 3X in Figure 2B. Then, the rock samples are scanned by Zeiss Xradia MICROXCT-400, shown in Figure 2C. One of the reconstructed three-dimensional rock images is shown in Figure 2D (the detailed reconstructed procedure has been presented in our former publication[6]). Following that, the micro-indentation test of sandstone sample is conducted by MFT-4000 multifunctional material performance tester, which is produced by Lanzhou Institute of Chemical Physics, Chinese Academy of Sciences. A conical indenter with flat tip is adopted, whose tip angle is 120° and the radius of the tip is 100 μm. The micro-indentation test is conducted in the center of the scanned samples, as the red mark shown in Figure 2D. All experiments are executed in the State Key Laboratory of Oil and Gas Reservoir Geology and Exploitation (SKLOGRGE) at Southwest Petroleum University, Chengdu, China.

The curve of indentation force vs the penetration depth with a displacement control is shown in Figure 3. The blue dot lines represent for the feature point of $h = 10$ and 15 μm in the study. Using Equations (1)-(5), the microscale elasticity of S1 is determined to be 17.8 GPa.

(2) Simulation on micro-indentation test

The pore scale rock matrix model is extracted and reconstructed from the micro-CT images. Considering that the radius and the maximum penetration depth are 100 μm and 15 μm, the size of the reconstructed rock model is 750 × 750 × 375 μm. The conical indenter with a flat punch is established in Abaqus software. The rock and indenter models are assembled and meshed using MIMICS software, as is shown in Figure 4.

The indentation simulation is conducted using the commercial software ANSYS. The mechanical behavior between the rock surface and the indenter is assumed to obey

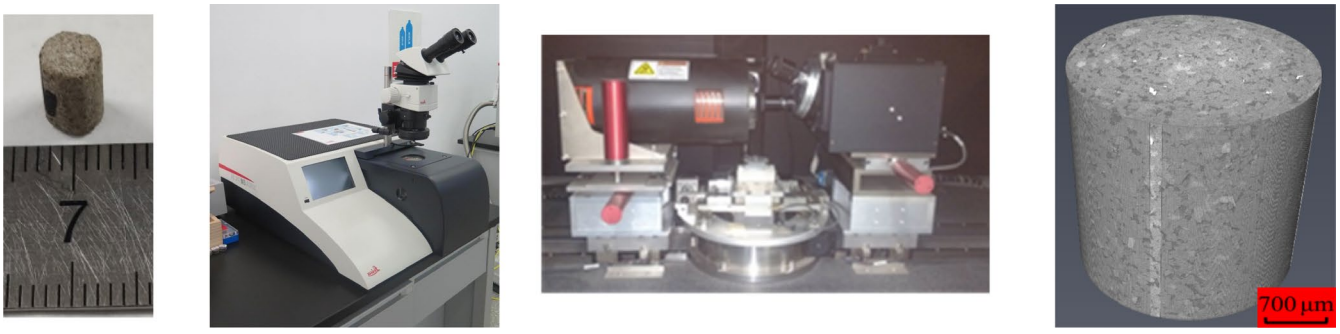

FIGURE 2 Sample preparation and the equipment used in this study

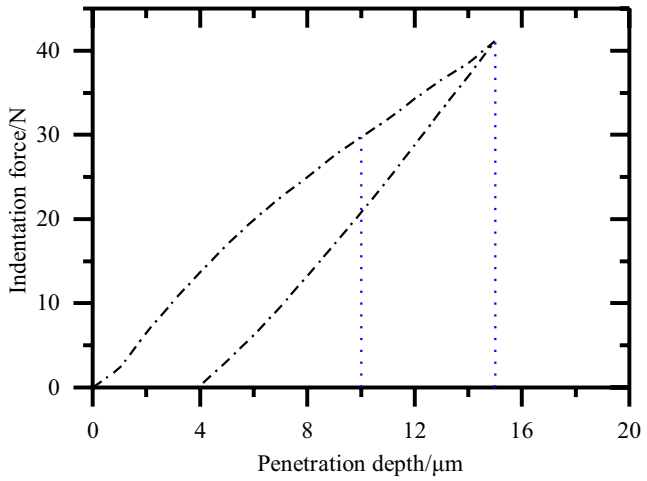

FIGURE 3 Indentation force vs the penetration depth

Coulomb's law, and the friction coefficient ν_f of 0.15 is used. Poisson's ratio acquired by the traditional biaxial compression test is employed. These two parameters are usually regarded to have a very slight effect on the indentation analysis.[45,51] As is stated in Section 2.2, the rock skeleton is an elastic-perfectly plastic material with Mohr-Coulomb yield criterion. Considering that there is no grain broken into the finer rock fragmentation, the internal friction angle φ is assumed to be constant before and after reaching the peaking point, which is obtained from the biaxial test on standard rock samples. The target cohesion force C is assumed to be varying from 14 MPa to 18.5 MPa, the range of which is based on that of the biaxial test. The ratio of the residual cohesion force C_r/C ranges from 0.3 to 0.65, which covers most of the rock materials. For sample S1, the detailed properties used in the simulation are shown in Table 1.

FIGURE 4 Reconstructed rock matrix and indentation model: (A) is the conical indenter with flat punch and (B) is the assembled indenter and rock matrix

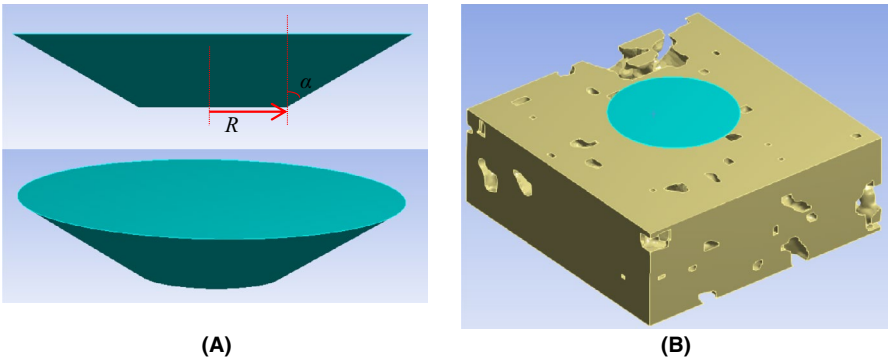

TABLE 1 Mechanical properties of rock S1 used in the indentation simulation

Young's modulus E/GPa	Poisson's ratio/ν	Internal friction angle φ/°	Cohesion force C/MPa	C_r/C
17.8	0.3	46	[14, 18.5]	[0.3, 0.65]

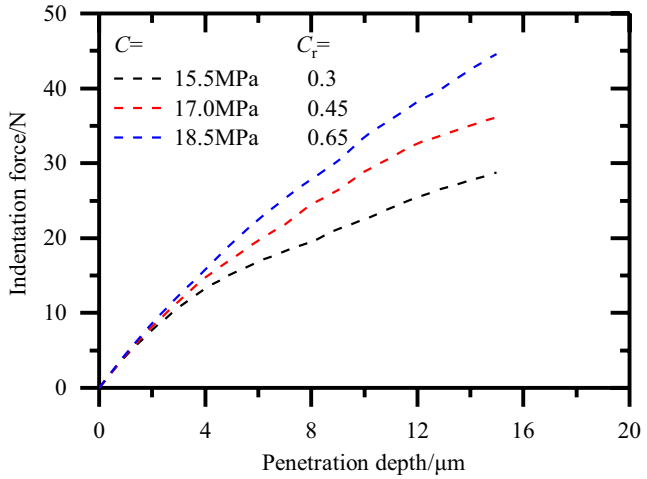

FIGURE 5 Typical penetration curve of sample S1 with different strength

The penetration curves of 56 cases (in combination of 7 values of C (14.0, 14.75, 15.5, 16.25, 17.0, 17.75, 18.5 MPa) with 8 values of Cr/C (0.30, 0.35, 0.40, 0.45, 0.50, 0.55, 0.60, 0.65)) are simulated on model S1 in this study, three of which are shown in Figure 5. Using these computational curves, the values of $W_{(h=10)}$ and $W_{(h=15)}$ can be determined, and the relationship curves between W/Ch^3 and C_r/E are acquired and shown in Figure 6. It is found that W/Ch^3 decreases with the rising of C/E monotonically, and the trend is dependent on C_r/C. The polynomial functions have been adopted to model the relationship between W/Ch^3 and C/E of the curves in Figure 6. The basic expression of the polynomial function is:

$$y = a_n x^n + a_{n-1} x^{n-1} + \cdots + a_2 x^2 + a_1 x + a_0 \quad (12)$$

TABLE 3 Fitted coefficients of A1-A4 for sample S1 in Equation (12)

C_r/C	A_1	A_2	A_3	A_4	R^2
(a) $h/R = 0.1$					
0.3	22.16209	9.47943	1.35092	0.06412	0.99909
0.35	21.51197	9.22948	1.31927	0.0628	0.9991
0.4	28.44073	12.20165	1.74425	0.08306	0.99842
0.45	32.3675	13.87848	1.98291	0.09438	0.99812
0.5	30.59419	13.12187	1.87527	0.08927	0.99847
0.55	28.86454	12.35408	1.76177	0.08368	0.99888
0.6	29.27845	12.54496	1.79095	0.08516	0.99885
0.65	24.40938	10.44605	1.48933	0.07071	0.99932
(b) $h/R = 0.15$					
0.3	12.59101	5.4104	0.77454	0.03693	0.99902
0.35	14.1728	6.10228	0.87534	0.04182	0.99873
0.4	15.47887	6.65299	0.95277	0.04545	0.99851
0.45	18.11635	7.78475	1.11466	0.05317	0.99795
0.5	22.04308	9.44551	1.34872	0.06416	0.99767
0.55	22.57485	9.66156	1.37788	0.06546	0.99787
0.6	20.32178	8.69793	1.24048	0.05893	0.99847
0.65	19.92019	8.52655	1.21608	0.05777	0.99864

where n is a non-negative integer that defines the degree of the polynomial. The coefficients of a_0-a_n are fitted using ORIGIN software with a known n. The correlation factor, R^2, is adopted to evaluate the fitting accuracy. The R^2 of $n = 2, 3, 4$ are listed in Table 2, in which $n = 3$ is satisfying for both accuracy and concision. Thus, the cubic polynomial functions are adopted in this paper,

$$\frac{W}{Ch^3} = A_4\left[\ln\left(\frac{C}{E}\right)\right]^3 + A_3\left[\ln\left(\frac{C}{E}\right)\right]^2 + A_2\left[\ln\left(\frac{C}{E}\right)\right] + A_1 \tag{13}$$

The fitted coefficients of A1-A4 are presented in Table 3. With these fitted functions of Equation (12), it is available to use the experimental results of W/Ch^3 ($h = 10$) and W/Ch^3 ($h = 15$) to obtain the corresponding C_r/C value. Two sets of values for W/Ch^3 vs C_r/C are deduced, and the two relationships can be illustrated. Figure 7 shows the example for sample S1. Two lines with different slope intersect at one point (marked by +). This intersecting point is the expected value of the cohesion force C and the residual ratio of the cohesion force (C_r/C), which is 17.95 MPa and 0.563. The complete workflow of the analysis procedure is presented in Figure 8.

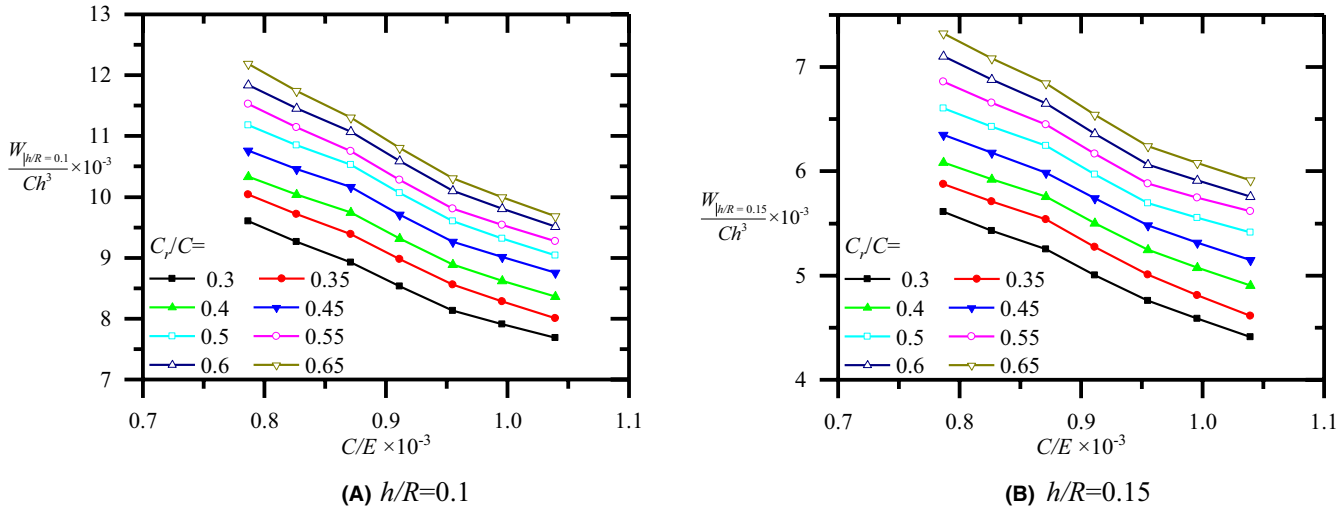

FIGURE 6 Relationship between W/Ch^3 and C/E under different strength for $h/R = 0.1$ (A) and 0.15 (B)

TABLE 2 R^2 of polynomial function fitting with $n = 2$, 3, or 4 for sample S1 in Equation (12)

	R^2					
	$h/R = 0.1$			$h/R = 0.15$		
C_r/C	$n = 2$	$n = 3$	$n = 4$	$n = 2$	$n = 3$	$n = 4$
0.3	0.99669	0.99909	0.99914	0.99654	0.99902	0.99913
0.35	0.99674	0.99910	0.99917	0.99562	0.99873	0.9989
0.4	0.99402	0.99842	0.99855	0.99457	0.99851	0.99867
0.45	0.99275	0.99812	0.99825	0.99555	0.99795	0.99927
0.5	0.99419	0.99847	0.99858	0.99087	0.99767	0.99781
0.55	0.99583	0.99888	0.99894	0.99175	0.99787	0.99798
0.6	0.99571	0.99885	0.99893	0.99419	0.99847	0.99855
0.65	0.99758	0.99932	0.99936	0.99285	0.99864	0.99871

3 | RESULTS

The pore scale uniaxial compression simulation on the reconstructed RVE and the uniaxial compression experiment on parallel samples are conducted, the results of which are used to validate the feasibility and applicability of the proposed methods. Five sandstone samples are adopted, among which, S1-S4 are natural sandstone samples, and S5 is synthetic samples with quartz grains by 3D printing. To reach the compromise between the representative property and the computation efficiency, the RVE analysis of the rock skeleton on the mechanical parameters against the model size is conducted using ANSYS software. RVE is the smallest subvolume of the heterogeneous material to be used in determining the corresponding effective properties for the macroscopic model.[52] As is shown in Figure 9A, the cubic from 100 to 400 pixels is extracted from the center of the original three-dimensional cylindrical rock image, which is gradually expanded to the surrounding area. The displacement loading is used to simulate the pore scale uniaxial compression along the z direction. As it is shown in Figure 9B, both Young's modulus and Poisson's ratio of model S1 approach to be steady when the volume size is beyond 300 pixels. Thus, the RVE for sample S1 is 300 pixels. Through the same methods, the RVE size of five sandstone samples is determined and presented in Table 3. As is stated before, Poisson's ratio and friction angle are obtained by the biaxial experiments on parallel samples, Young's modulus is acquired by micro-indentation experiments, and the initial cohesion force and residual cohesion

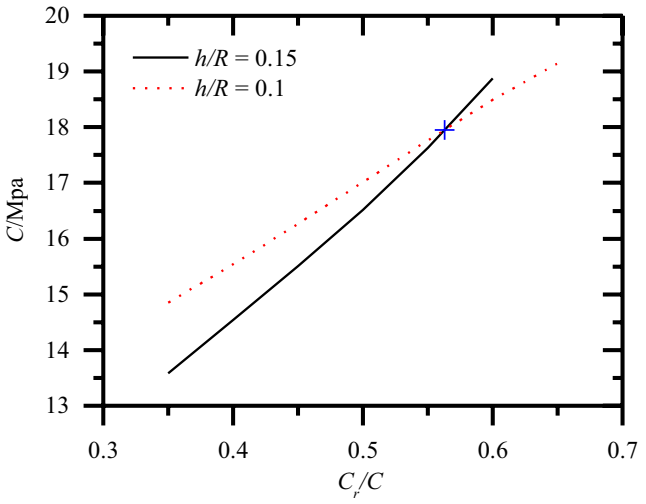

FIGURE 7 Identification of the estimated solution as being the interaction of the two curves (from Equation (13) with Table 2 (h/R-0.1 and 0.15))

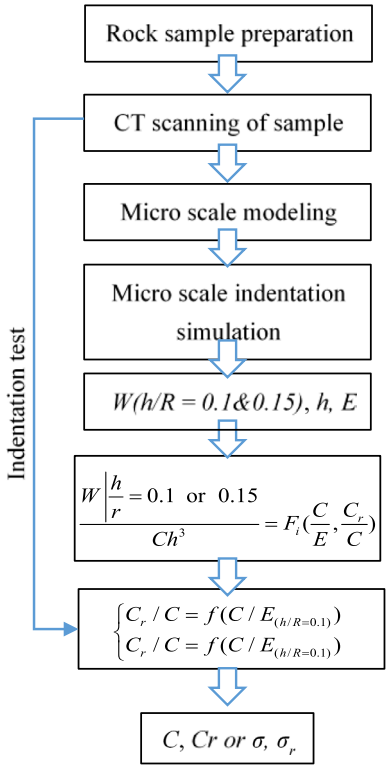

FIGURE 8 Schematic of micro scale elastoplastic properties evaluation

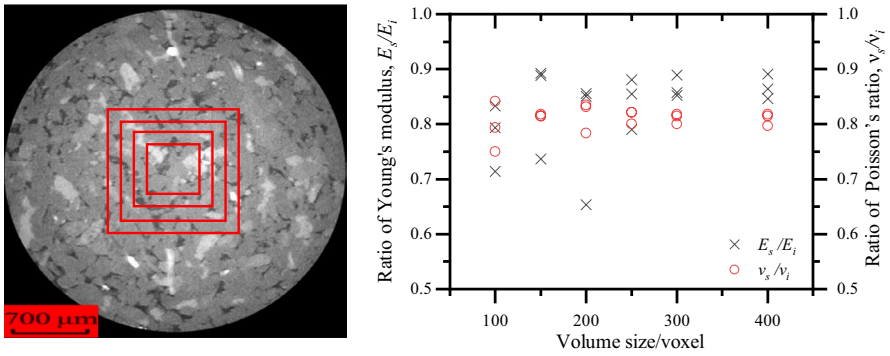

FIGURE 9 RVE analysis of mechanical properties microstructure: (A) is the model selection for REV analysis and (B) is the ratio of Young's modulus and ratio of Poisson's ratio against model size for the RVE analysis, where the subscript *s* and *i* represent the calculated results of the model and the input parameters

TABLE 4 Parameters of the five samples used in the simulation

Sample	Elements number	Porosity/%	Length/mm	REV/pixel	Young's modulus/GPa	Poisson's ratio	Friction angle/°	Initial cohesion force/MPa	Residual cohesion force/MPa
S1	1 744 435	9.07	0.63	300^3	17.83	0.3	46	18.0	10.1
S2	2 787 997	17.6	1.3	300^3	19.10	0.26	34	23.4	9.7
S3	797 051	20.3	1.0	300^3	24.90	0.21	23	24.7	11.2
S4	2 072 375	38.6	0.75	400^3	9.80	0.32	24	19.2	12.0
S5	1 812 356	40.6	1.748	300^3	5.59	0.15	14	7.13	3.02

force are determined using the methods proposed in Section 2.3. These mechanical parameters are also listed in Table 4.

In the uniaxial compression simulation, the boundary conditions of the displacement loading and support are applied to the top and bottom surface of the model along the *z* direction, respectively. The surrounding surfaces are unconstrained, which is the same as the experiment. A maximum displacement with the same strain of the uniaxial compression experiment is adopted. The plastic strain distribution of samples S1, S3, and S5 in the simulation and the failure mode after uniaxial compression experiment are presented in Figure 10. In Figure 10A, sample S1 breaks by the typical shear failure mode with a single fracture surface, and there is also a plastic surface in the simulation result. In Figure 10B, sample S3 fails by the *X* shape conjugate shear fracture, and an *X* shape conjugate plastic plane is also observed in one side of the model in the simulation result. In Figure 10C, the synthetic sandstone is damaged by the tensile fracture, and there is a plastic plane through the top surface in the simulation. The failure of the samples presented in this paper covers the most fracture modes of rock in uniaxial compression experiments. Since the perfectly plastic material is assumed, the facture in the experiment is presented in the elastic-perfectly plastic region. The results verify the representativeness and feasibility of the simulation on the reconstructed RVE models.

The stress-strain curves of the uniaxial compression simulation and experiment on the five sandstone samples are shown in Figure 11. The standard core (with the size of Φ2.5 × 5 cm) for the experiments is drilled from the same original rock samples as the small cores used for micro-CT scanning and micro-indentation test. The linear elasticity part of the curves in the simulation agrees well with the experimental results. The nonlinear part of the uniaxial compression strength shows relative discreteness compared with the experimental results. The maximum deviation of the uniaxial compression strength (UCS) is observed for sample S2 as −12.49%. The main reason lies in that the pore structure of the small sample for simulation is not exactly same as the standard sample for experiment. Though the two samples are drilled from the same original rock core, the heterogeneity of the rock pore structure leads to the deviation of the stress-strain curves. Meanwhile, the microscale sandstone skeleton is assumed as isotropic and homogeneous with perfectly elastic-plastic behaviors. The assumption means that the rock in the simulation does not crack as the experiments when the shear stress of the model exceeds the value defined by the Mohr-Coulomb criterion. In consideration of these reasons, the deviation is in an acceptable range.

Furthermore, as is listed in Table 5, Young's modulus and UCS of the reconstructed models are lower than the input parameters of the rock skeleton. The rock can be regarded as a kind of composite material made up by two phases, where the mechanical strength of the pore is 0. According to the rule in literature,[53] Young's modulus is in the range of $\left[\left(\frac{\phi}{E_p}+\frac{1-\phi}{E_s}\right)^{-1},(1-\phi)E_s\right]$, where ϕ is the porosity, and E_s and

FIGURE 10 Plastic strain distribution in the simulation and failure mode after uniaxial compression experiment

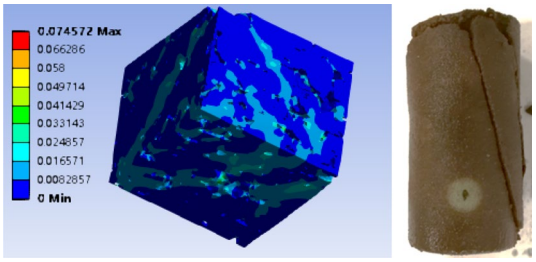

(A) Plastic strain distribution of S1 in the simulation and shear fracture after uniaxial compression experiment

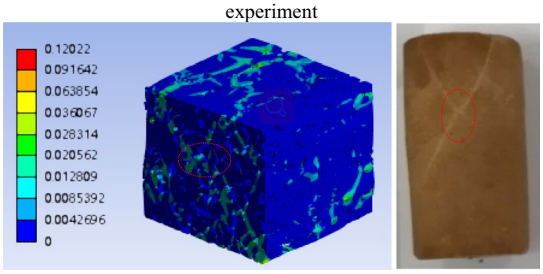

(B) Plastic strain distribution of S3 in the simulation and *X* shape shear fracture after uniaxial compression experiment

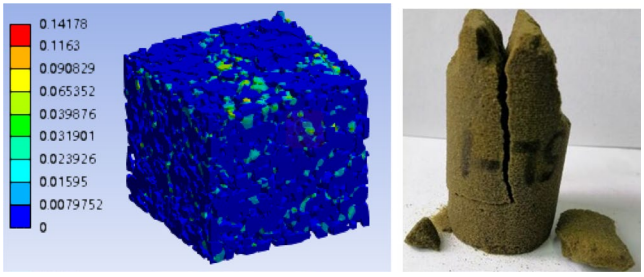

(C) Plastic strain distribution of S5 in the simulation and tensile fracture after uniaxial compression experiment

E_p are Young's modulus of the rock skeleton and pore, respectively. Thus, the lower bound of Young's modulus of the model approaches to zero. It is found that Young's modulus of the reconstructed model is within this interval. These results prove the feasibility of the proposed method in this paper.

4 | CONCLUSIONS

This paper develops a novel method to determine the microscopic initial strength and residual strength of brittle sandstone using the micro-indentation test and simulation, which deals with the elastic-perfectly plastic rock with known constitutive model and pore scale structure.

The dimensionless analysis on the micro-indentation curve of rock is conducted using Buckingham's PI theorem. The key influencing factors of the elastoplastic properties (including the initial cohesive force and the residual cohesive force) on the indentation curve are determined. Based on the dimensionless analysis results, the proposed method is conducted. Firstly, small cylindrical rock samples are prepared for micro-CT scanning and micro-indentation test. The indentation curve and microscale Young's modulus are acquired using the indentation test. The microscopic structure of rock is established from the micro-CT image and used as input for the micro-indentation simulation. Then, the function between the indentation curve and strength is deduced by the parametric FEM study on the pore scale indentation simulation. Using this function, the microscale initial strength and residual strength of the brittle sandstone are evaluated.

This method is validated by comparing the microscale numerical simulation of uniaxial compression on the RVE of rock with the experimental results of the corresponding samples. Meanwhile, typical fracture modes on the RVE simulation for uniaxial compression, including shear fracture, *X* shape shear fracture, and tensile fracture, are investigated and compared with the experimental results. A reasonable deviation of the experimental stress-strain curves, Young's modulus, and uniaxial compression strength from those of the RVE simulation results is observed and analyzed. Although the brittle sandstone is adopted in this study, the proposed analyzing methods can be applied for all kinds of rocks with known constitutive model and pore scale structure.

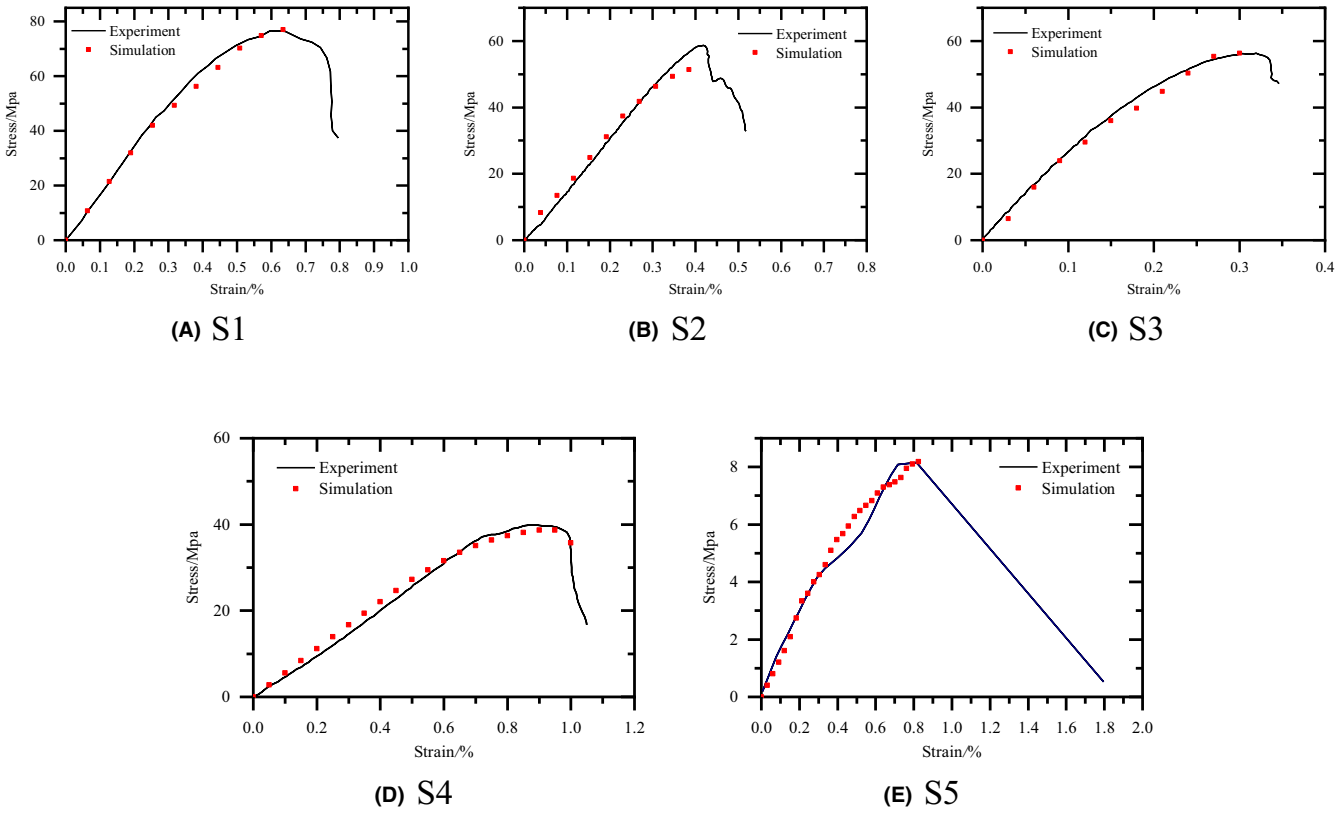

FIGURE 11 Stress-strain curves of the uniaxial compression simulation and experiment

TABLE 5 Young's modulus and UCS of the reconstructed models and the input values of rock skeleton

Sample	Young's modulus/GPa		Young's modulus/GPa		UCS/MPa	
	Model	Input	Lower bound	Upper bound	Model	Input
S1	15.20	17.83	0	16.21	76.41	89.05
S2	14.49	19.10	0	15.74	56.36	87.99
S3	17.61	24.90	0	19.85	56.31	99.04
S4	5.43	12.60	0	6.02	38.67	59.12
S5	2.78	5.59	0	3.35	8.18	18.26

ACKNOWLEDGMENTS

This work is supported by the Open Research Fund of State Key Laboratory of Geomechanics and Geotechnical Engineering, Institute of Rock and Soil Mechanics, Chinese Academy of Sciences (Grant No. Z017009); National Natural Science Foundation of China (Grant No. 51909225); National Science and Technology Major Project of China (Grant No. 2017ZX05013001-002); and the China Scholarship Council. We also acknowledge the financial support of King Abdullah University of Science and Technology (KAUST) through the grant No. BAS/1/1351-01 and the National Natural Science Foundation of China through the grant No. 51874262.

ORCID

Rui Song https://orcid.org/0000-0002-5439-5760
Yao Wang https://orcid.org/0000-0002-7124-7671
Mengmeng Cui https://orcid.org/0000-0001-7857-5582

REFERENCES

1. Rong H, Qian CX, Li LZ. Study on microstructure and properties of sandstone cemented by microbe cement. *Constr Build Mater*. 2012;36:687-694.
2. Yang SQ, Jing HW, Wang SY. Experimental investigation on the strength, deformability, failure behavior and acoustic emission locations of red sandstone under triaxial compression. *Rock Mech Rock Eng*. 2012;45(4):583-606.

3. Lei R, Wang Y, Zhang L, et al. The evolution of sandstone microstructure and mechanical properties with thermal damage. *Energy Sci Eng*. 2019;7:3058-3075.
4. Bjorlykke K. *Petroleum Geoscience: From Sedimentary Environments to Rock Physics*. Berlin, Germany: Springer Science & Business Media; 2010.
5. Lai J, Wang G, Wang S, et al. Review of diagenetic facies in tight sandstones: diagenesis, diagenetic minerals, and prediction via well logs. *Earth Sci Rev*. 2018;185:234-258.
6. Song R, Liu J, Cui M. A new method to reconstruct structured mesh model from micro-computed tomography images of porous media and its application. *Int J Heat Mass Transf*. 2017;109:705-715.
7. Song R, Cui M, Liu J. Single and multiple objective optimization of a natural gas liquefaction process. *Energy*. 2017;124:19-28.
8. Song R, Wang Y, Liu J, Cui M, Lei Y. Comparative analysis on pore-scale permeability prediction on micro-CT images of rock using numerical and empirical approaches. *Energy Sci Eng*. 2019;7:2842-2854.
9. Ju Y, Wang H, Yang Y, Hu Q, Peng R. Numerical simulation of mechanisms of deformation, failure and energy dissipation in porous rock media subjected to wave stresses. *Sci Chin Technol Sci*. 2010;53(4):1098-1113.
10. Liu J, Sarout J, Zhang M, Dautriat J, Veveakis E, Regenauer-Lieb K. Computational upscaling of Drucker-Prager plasticity from micro-CT images of synthetic porous rock. *Geophys J Int*. 2017;212(1):151-163.
11. Zhou XP, Xiao N. A novel 3D geometrical reconstruction model for porous rocks. *Eng Geol*. 2017;228:371-384.
12. Zhou XP, Xiao N. Analysis of fracture properties of three-dimensional reconstructed rock model using hierarchical-fractal annealing algorithm. *Eng Geol*. 2019;256:39-56.
13. Song R, Cui M, Liu J, Ranjith PG, Lei Y. A pore-scale simulation on thermal-hydromechanical coupling mechanism of rock. *Geofluids*. 2017;2017:1-12.
14. Hashin Z, Shtrikman S. A variational approach to the theory of the elastic behaviour of multiphase materials. *J Mech Phys Solids*. 1963;11(2):127-140.
15. Song R, Peng J, Sun S, Wang Y, Cui M, Liu J. Visualized experiments on residual oil classification and its influencing factors in waterflooding using micro-computed tomography. *J Energy Res Technol*. 2020;142(8):83003.
16. Weddfelt K, Saadati M, Larsson PL. On the load capacity and fracture mechanism of hard rocks at indentation loading. *Int J Rock Mech Min Sci*. 2017;100:170-176.
17. Lee H, Vimonsatit V, Chindaprasirt P. Mechanical and micromechanical properties of alkali activated fly-ash cement based on nano-indentation. *Constr Build Mater*. 2016;107:95-102.
18. Kumano A, Goldsmith W. An analytical and experimental investigation of the effect of impact on coarse granular rocks. *Rock Mech*. 1982;15(2):67-97.
19. Pang SS, Goldsmith W. Investigation of crack formation during loading of brittle rock. *Rock Mech Rock Eng*. 1990;23(1):53-63.
20. Samuels LE, Mulhearn TO. An experimental investigation of the deformed zone associated with indentation hardness impressions. *J Mech Phys Solids*. 1957;5(2):125-134.
21. Ladanyi B. Rock failure under concentrated loading. In: *The 10th US Symposium on Rock Mechanics (USRMS)*. American Rock Mechanics Association; 1968:363-387.
22. Jeng FS, Einstein HH, Whittle AJ, Germaine JT. *Deep Penetration into Frictional Ductile and Brittle Materials*. NASA STI/Recon Technical Report N, 93; 1992.
23. Yagiz S, Rostami J. Indentation test for the measurement of rock brittleness. In: *46th US Rock Mechanics/Geomechanics Symposium*. American Rock Mechanics Association; 2012.
24. Chen L, Labuz J. Normal wedge indentation of rocks by a wedge-shaped tool III: experimental evidence. *Int J Rock Mech Min Sci Geomech*. 1997;31(2):81-94.
25. Ortega JA, Ulm FJ, Abousleiman Y. The effect of the nanogranular nature of shale on their poroelastic behavior. *Acta Geotech*. 2007;2(3):155-182.
26. Zhang H, Huang G, Song H, Kang Y. Experimental investigation of deformation and failure mechanisms in rock under indentation by digital image correlation. *Eng Fract Mech*. 2012;96:667-675.
27. Brace WF. Behavior of rock salt, limestone, and anhydrite during indentation. *J Geophys Res*. 1960;65(6):1773-1788.
28. Mateus J, Saavedra N, Carrillo ZC, Mateus D. Correlation development between indentation parameters and uniaxial compressive strength for Colombian sandstones. *CT&F-Ciencia Tecnol Futuro*. 2007;3(3):125-136.
29. Diego H, Zuly C, Yair Q. Experimental correlations to obtain elastic properties of shale rocks using the indentation test. In: *ISRM Conference on Rock Mechanics for Natural Resources and Infrastructure-SBMR 2014, November*. International Society for Rock Mechanics and Rock Engineering; 2014.
30. Sulem J, Cerrolaza M. Finite element analysis of the indentation test on rocks with microstructure. *Comput Geotech*. 2002;29(2):95-117.
31. Alehossein H, Detournay E, Huang H. An analytical model for the indentation of rocks by blunt tools. *Rock Mech Rock Eng*. 2000;33(4):267-284.
32. Huang HY, Lecampion B, Detournay E. Discrete element modeling of tool-rock interaction I: rock cutting. *Int J Numer Anal Meth Geomech*. 2013;37(13):1913-1929.
33. Rahal S, Sellier A, Verdier J. Modelling of change in permeability induced by dilatancy for brittle geomaterials. *Constr Build Mater*. 2016;125:613-624.
34. Gabsi N, Souissi S, Hamdi E, Karrech A. Micro-mechanical damage model for geomaterials behavior under indentation. In: *1st International Conference on Advances in Rock Mechanics-TuniRock 2018*. International Society for Rock Mechanics and Rock Engineering; 2018.
35. Kou SQ, Huang Y, Tan XC, Lindqvist PA. Identification of the governing parameters related to rock indentation depth by using similarity analysis. *Eng Geol*. 1998;49(3-4):261-269.
36. Abedi S, Slim M, Hofmann R, Bryndzia T, Ulm FJ. Nanochemo-mechanical signature of organic-rich shales: a coupled indentation–EDX analysis. *Acta Geotech*. 2016;11(3):559-572.
37. Wang W, Xu WD. A new method of testing rock properties. *Rock Soil Mech*. 2009;S1:538-544 (in Chinese).
38. Auvray C, Lafrance N, Bartier D. Elastic modulus of claystone evaluated by nano-/micro-indentation tests and meso-compression tests. *J Rock Mech Geotech Eng*. 2017;9(1):84-91.
39. Han Q, Chen P, Ma T. Influencing factor analysis of shale micro-indentation measurement. *J Nat Gas Sci Eng*. 2015;27:641-650.
40. Zhu W, Hughes JJ, Bicanic N, Pearce CJ. Nanoindentation mapping of mechanical properties of cement paste and natural rocks. *Mater Charact*. 2007;58(11-12):1189-1198.

41. Daphalapurkar NP, Wang F, Fu B, Lu H, Komanduri R. Determination of mechanical properties of sand grains by nanoindentation. *Exp Mech*. 2011;51(5):719-728.
42. Goodarzi M, Rouainia M, Aplin AC. Numerical evaluation of mean-field homogenisation methods for predicting shale elastic response. *Comput Geosci*. 2016;20(5):1109-1122.
43. Sneddon IN. The relation between load and penetration in the axisymmetric Boussinesq problem for a punch of arbitrary profile. *Int J Eng Sci*. 1965;3(1):47-57.
44. Oliver WC, Pharr GMJ. An improved technique for determining hardness and elastic modulus using load and displacement sensing indentation experiments. *J Mater Res*. 1992;7(06):1564-1583.
45. Cheng YT, Cheng CM. Scaling, dimensional analysis, and indentation measurements. *Mater Sci Eng: R: Rep*. 2004;44(4-5):91-149.
46. Phadikar JK, Bogetti TA, Karlsson AM. On the uniqueness and sensitivity of indentation testing of isotropic materials. *Int J Solids Struct*. 2013;50(20-21):3242-3253.
47. Akahori T, Nagakura T, Fushimi S, Yonezu A. An indentation method for evaluating the residual stress of polymeric materials: equi-biaxial and non-equi-biaxial residual stress states. *Polym Testing*. 2018;70:378-388.
48. Renani HR, Martin CD. Cohesion degradation and friction mobilization in brittle failure of rocks. *Int J Rock Mech Min Sci*. 2018;106:1-13.
49. Walton G. Initial guidelines for the selection of input parameters for cohesion-weakening-friction-strengthening (CWFS) analysis of excavations in brittle rock. *Tunn Undergr Space Technol*. 2019;84:189-200.
50. Buckingham E. On physically similar systems; illustrations of the use of dimensional equations. *Phys Rev*. 1914;4(4):345.
51. Chen X, Ogasawara N, Zhao M, Chiba N. On the uniqueness of measuring elastoplastic properties from indentation: the indistinguishable mystical materials. *J Mech Phys Solids*. 2007;55(8):1618-1660.
52. Nemat-Nasser S, Hori M. *Micromechanics: Overall Properties of Heterogeneous Materials*. Amsterdam, The Netherlands: Elsevier; 2013.
53. Voigt W. Ueber die Beziehung zwischen den beiden Elasticitätsconstanten isotroper Körper. *Ann Phys*. 1889;274(12):573-587.

How to cite this article: Song R, Wang Y, Sun S, Cui M, Liu J. Evaluation of elastoplastic properties of brittle sandstone at microscale using micro-indentation test and simulation. *Energy Sci Eng*. 2020;00:1–12. https://doi.org/10.1002/ese3.759